https://doi.org/10.5194/egusphere-2024-1813
Preprint. Discussion started: 20 June 2024

National Weather Service Alaska Sea Ice Program: Gridded ice concentration maps for the Alaskan Arctic

Astrid Pacini[1], Michael Steele[1], Mary-Beth Schreck[2]

[1]University of Washington Applied Physics Laboratory, Seattle, WA, 98105, USA
[2]National Weather Service Alaska Sea Ice Program, Anchorage, AK, 99513, USA

Correspondence to: Astrid Pacini (apacini@uw.edu)

Abstract. There are many challenges associated with obtaining high-fidelity sea ice concentration (SIC) information, and products that rely solely on passive microwave measurements often struggle to represent conditions at low concentration, especially within the Marginal Ice Zone and during periods of active melt. Here, we present a new SIC product for the Alaskan Arctic generated by the National Weather Service Alaska Sea Ice Program (hereafter referred to as ASIP) that synthesizes a variety of satellite SIC and in-situ observations from 2007-present. These SIC fields have been primarily used for operational purposes and have not yet been gridded or independently validated. In this study, we first grid the ASIP product into 0.05° resolution in both latitude and longitude. We then perform extensive intercomparison with an international database of ship-based in-situ SIC observations, supplemented with observations from Saildrones. Additionally, an intercomparison between three ice products is performed: (i) ASIP, (ii) a high-resolution passive microwave product (AMSR2), and (iii) an operational product available from the National Snow and Ice Data Center that originates at the National Ice Center (MASIE). This intercomparison demonstrates that all products perform similarly when compared to in-situ observations generally, but ASIP outperforms the other products during periods of active melt and in low SIC regions. Furthermore, we show that the similarity in performance among products is due to the in-situ asset distribution, as most in-situ observations are far from the ice edge in locations where all products agree. We find that the ASIP ice edge is generally farther south than both the AMSR2 and MASIE ice edges, by an average of approximately 55 km in the winter and 175 km in summer for ASIP vs. AMSR2, and 60 km in the winter and 130 km in the summer for ASIP vs. MASIE.

Key Points:

1. ASIP is an operational, mostly remote sensing-based sea ice dataset for the Alaskan Arctic that has not previously been gridded nor independently validated. Here we describe how the data are parsed, gridded, and validated against

https://doi.org/10.5194/egusphere-2024-1813
Preprint. Discussion started: 20 June 2024

a relatively under-utilized in-situ sea ice concentration dataset. These in situ data are also used for validation with two other satellite-based products: AMSR2 and MASIE.

2. All three products considered (ASIP, AMSR2, MASIE) perform similarly when compared against in-situ observations when the full SIC range 0-100% is considered.
3. For the Marginal Ice Zone (MIZ; SIC>=15% & <=80%), ASIP performs better than AMSR2 at predicting the presence of ice; MASIE has by definition no information at SIC < 40%. In the MIZ, ASIP tends to over-predict SIC, while AMSR2 under-predicts SIC by a larger amount.
4. We find that the ASIP ice edge is on average farther south than both the AMSR2 and MASIE ice edges, with no systematic differences as a function of longitude in the Alaskan Arctic.

1 Introduction

The significant change in Arctic sea ice cover over the last century is a clear indicator of the effects of anthropogenic greenhouse gas emissions on our high-latitude oceans (e.g. Fox-Kemper et al., 2021). Strong reductions in sea ice extent and thickness, changes in ice age (from multi-year ice to seasonal ice), and changes in ice drift and deformation characterize the modern record (e.g., Haine and Martin, 2017; Perovich et al., 2020). Serreze and Stroeve (2015) demonstrated that September sea ice extent is decreasing at a rate of 13.3% per decade over the satellite record, and they argued that this trend is accelerating due to feedback loops within the Arctic. Synchronously, the mean ice thickness has decreased from 3.20 m (1958-1976) to 1.43 m (2003-2007) (Kwok and Rothrock, 2009; Lindsay and Schweiger, 2015; Haine and Martin, 2017). Beyond the physical and ecosystem impacts of these trends, changes in sea ice are altering the operational and research environments for ships transiting the Arctic Ocean and its marginal seas; increased shipping is occurring along both the Northwest Passage and the Northern Sea Route (e.g. Arctic Council, 2009; Boylan, 2021), which in turn necessitates increased infrastructure in the region for safety and governance. At the very basic level, these ships need reliable ice maps to inform routing decisions. However, despite the clear trends in Arctic sea ice and the need to measure these changes, there are many challenges associated with obtaining high-fidelity measurements of sea ice concentration (SIC). This is especially true in low concentration environments and during periods of active melt (e.g. Kern et al., 2020).

Historically, there have been two main approaches to measuring SIC from satellite: passive microwave measurements and the use of other imagery. The former provides a continuous, near-daily record of ice conditions in polar regions since October 1978; as such, passive microwave is a powerful tool for diagnosing and analysing the long-term evolution of ice, as a consistent processing algorithm can be applied to a consistent observational record (e.g. Meier et al., 2015). There are numerous algorithms and quality-control methodologies in place to processes these measurements of brightness temperature (e.g. Cavalieri et al., 1984, 1999; Comiso, 1986; Comiso and Nishio, 2008). However, a key challenge to brightness temperature

https://doi.org/10.5194/egusphere-2024-1813
Preprint. Discussion started: 20 June 2024

measurements is the inability of these measurements to distinguish between melt water on the surface of ice, leads in the ice, and open water conditions (e.g. Kern et al., 2020; Meier and Notz, 2010; Gogineni et al., 1992; Grenfell and Lhanick, 1985). This results in an underestimation of sea ice extent during periods of active melt, especially in summer months (e.g. Kern et al., 2020; Ivanova et al., 2015; Rösel et al., 2012b; Markus and Dokken, 2002; Comiso and Kwok, 1996; Steffan and Schweiger, 1991; Cavalieri et al., 1990).

The second method for obtaining ice concentration information from satellite is the use of other methods, e.g. active sensors such as scatterometers and synthetic aperture radar, and passive sensors such as optical and visible imagery. These data are synthesized, and sometimes merged with passive microwave measurements, to make up a second class of ice concentration measurements known as operational ice charts. Operational maps are generated by an analyst using available imagery, but they are not consistent over the historical record due to improvements in satellite technology, the availability of clear imagery (often dependent on cloud and weather conditions), and changes in analyst personnel (e.g. Kern et al., 2020). Operational charts can be higher resolution than their passive microwave counterparts and may better represent summertime conditions owing to their use of multiple satellite products. While passive microwave can provide insight on long term trends, operational products can describe in high resolution the daily state of the sea ice pack. For example, in the field, operational stakeholders rely on these data to decide on ship routes and instrumentation deployment locations; in research, these maps provide valuable high-resolution information for summertime conditions and small-scale dynamics (e,g, Chiodi et al., 2021). Operational ice maps can also be a valuable tool for driving operational models and weather predictions (e.g. Meier et al., 2015), although most large-scale users rely on low-latency SIC fields from passive microwave (e.g. Chin et al., 2017). As with passive microwave products, there are many processing agencies and techniques used to generate operational ice maps. For example, Agnew and Howell (2003) compare weekly operational Canadian Ice Service sea-ice charts with passive microwave data derived using the NASA Team algorithm to show that the NASA Team algorithm underpredicts sea ice area in the Canadian Arctic by 20.5 – 33.5% during summer melt periods, and by 7.6 – 43.5% in the fall while ice is growing. Another study by Meier et al. (2015) compares passive microwave measurements against Multisensor Analyzed Sea Ice Extent (MASIE), an operational product generated by the US National Ice Center (NIC) (US National Ice Center et al., 2010). They show that MASIE produces a higher-resolution ice edge compared with the passive microwave ice edge, and that sea ice extent from MASIE is generally larger than that derived from passive microwave.

In this study, we present an operational SIC product for the Alaskan Arctic generated by the National Weather Service Alaska Sea Ice Program (hereafter referred to as ASIP). Our motivation comes in part from a case study of conditions in the Beaufort Sea on August 21, 2022 (Fig. 1). (The color scale used in all panels of Fig. 1 is standard World Meteorological Organization egg code for ice charts and is explained in further detail below.) During this time, the NASA Salinity and Stratification at the Sea Ice Edge field program was operating in the Pacific Arctic (Drushka et al., accepted). As part of the field program, four

https://doi.org/10.5194/egusphere-2024-1813
Preprint. Discussion started: 20 June 2024

remotely operated Wave Glider vehicles (Thomson, 2023) were deployed to obtain measurements of salinity near the sea ice edge. To do this successfully, there was a critical need for accurate daily ice edge information. Figure 1a depicts the ice concentration on August 21, 2022 from a 25 km resolution passive microwave dataset (AMSR2) that relies on the NASA Team 2 algorithm, obtained from the US NIC (Markus et al., 2018). This product shows compact ice north of 72°N, with pockets of open water found at 73°N, 150°W and 74.5°N, 146°W and open water west of 157°W and south of 72°N. AMSR2 data processed using the ASI algorithm (Fig. 1b; Spreen et al., 2008) at 3.125 km resolution show a similar ice distribution as in Fig 1a, although with higher spatial detail (including larger areas of open water within the pack). We compare these two passive microwave measurements with MASIE (Fig. 1c; US National Ice Center et al., 2010), which uses a binary ice flag to indicate either ice or open water and a 40% ice concentration cut-off (see details in section 2.3.2). Consistent with both AMSR2 products, MASIE indicates compact ice north of 72°N, although MASIE indicates the presence of ice to the west of 157°W. MASIE also predicts a region of ice to the east of Prudhoe Bay, extending south from the icepack toward Alaska near 71°N. Finally, ASIP (Fig. 1d) shows ice throughout the domain north of 72°N, consistent with MASIE. However, ASIP also identifies significantly more low-concentration ice at the southern boundary of the ice pack, including a tongue of ice extending toward the southeast in the direction of Prudhoe Bay. This tongue is not present in the three other products considered.

At this time the NASA SASSIE program deployed four Wave Gliders (Thomson et al., 2018) in the region. The positions of these autonomous assets for one week prior to, and one week after, these maps are shown in gray in Fig. 1. Figure 1e is an image taken during the Wave Glider deployment cruise onboard the RV Ukpik, demonstrating that ice was clearly present during the deployment, in agreement with ASIP and in disagreement with AMSR2 and MASIE. Furthermore, the presence of ice during deployment resulted in two Wave Gliders being deployed to the west of the tongue of ice at approximately 150°W and two to the east of this tongue. Despite efforts to join these tracks over the two weeks shown in the figure, the persistence of this ice tongue resulted in two separate survey regions. Therefore, it is clear that in this case, ASIP best represented the presence of low concentration ice near the Alaskan coast. A second motivation for investigating the use of ASIP was its superior performance in evaluating sea ice during a NASA-sponsored saildrone cruise in the northeast Chukchi Sea, also during summer 2022 (García-Reyes et al., 2023). These two field campaigns, in addition to the previously discussed increase in human activities near the Arctic ice pack, motivates this detailed investigation of the performance of ASIP in the Pacific Arctic more broadly.

The paper is structured as follows. First, we describe the parsing and gridding methodology, then we perform an intercomparison with in-situ measurements of sea ice, compare ASIP to a passive microwave product (AMSR2) and a second operational product (MASIE), and finally investigate the location of the ice edge in all three products.

https://doi.org/10.5194/egusphere-2024-1813
Preprint. Discussion started: 20 June 2024

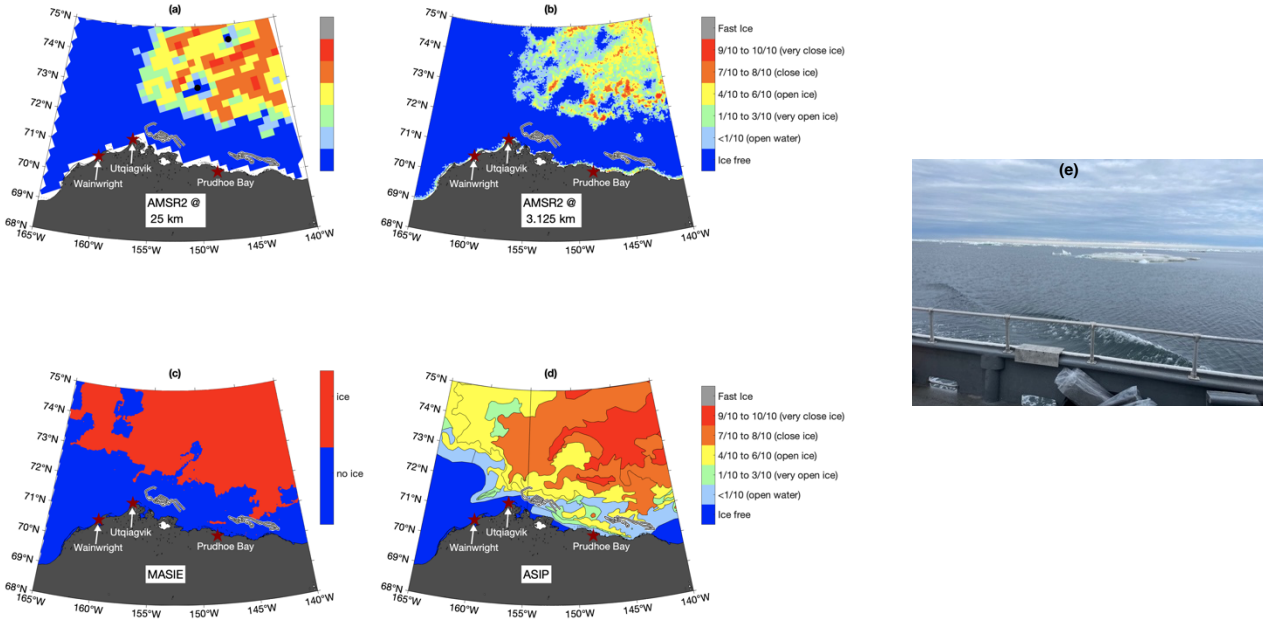

Figure 1: Sea ice conditions according to different ice products for August 21, 2022. (a) AMSR2 at 25 km resolution using the NASA Team 2 algorithm (Markus et al., 2018). (b) AMSR2 at 3.125 km using the ASI algorithm (Spreen et al., 2008). (c) MASIE ice/no ice (US National Ice Center et al., 2010). (d) National Weather Service Alaska Sea Ice Program. The track lines of four Wave Gliders operating in the region are overlaid in gray, representing the tracks for one week prior to one week post the ice images (Aug 14 – Aug 28, 2022). Note that WMO standard egg code colorbar is used in all four panels. Details of WMO egg code can be found in Section 2.1. For AMSR2 data, this required binning of individual grid cells into the WMO ranges. As such, data were rounded to the nearest ten digit to fall into respective concentration ranges. For example, a pixel with ice concentration of 35-60% would fall into the yellow band that represents 4/10 to 6/10 ice. (e) Image taken by Jim Thomson during the Wave Glider deployment cruise on August 12, 2022

2 Data and Methods

2.1 National Weather Service Alaska Sea Ice Program

The National Weather Service's Alaska Sea Ice Program provides real-time ice information for conditions in the Pacific Arctic (Heim and Schreck, 2017). This product is primarily operational; ASIP supports ships working in the region, including shipping and transportation vessels, the fishing fleet, the Coast Guard, tourist vessels, and research vessels. ASIP also supports Alaska native communities and subsistence hunts, the oil and gas industry, Alaska Fish & Wildlife, the Department of Homeland Security, and National Weather Service forecasters (Hufford, 2009; Deemer et al., 2017). ASIP issues a variety of products to stakeholders, including text-based and graphical information. Specifically, ASIP issues daily sea ice maps for the full domain (135°W – 175°E, 45°N – 80°N) and regional sectors, a 5-day graphical sea ice forecast, text-based sea ice forecasts

https://doi.org/10.5194/egusphere-2024-1813
Preprint. Discussion started: 20 June 2024

for five days into the future, including regional forecasts for the Beaufort, Chukchi, and Bering Seas, and a three-month sea ice outlook for the entire domain. Additionally, ASIP publishes a sea surface temperature analysis for the region.

The data are produced following World Meteorological Organization (WMO) standards for archiving digital ice charts (WMO, 1970). Specifically, all ice maps are presented as GIS Shapefiles following SIGRID-3 vector archive format. ASIP creates daily SIGRID-3 ice charts for Alaskan waters including the Beaufort Sea, Chukchi Sea, Bering Sea, and Cook Inlet. These SIGRID-3 files have two main components: the shapefile containing the ice analysis information (ice polygons and related attributes) and the metadata describing the ice analysis data under the SIGRID-3 format. The Sea Ice Analysis represents ice conditions valid at approximately 0030 UTC but is analyzed from imagery over the preceding 24 hours. Imagery utilized includes synthetic aperture radar (SAR), Polar Orbiter Satellite (POES) visible and infrared imagery such as Visible Infrared Imaging Radiometer Suite (VIIRS), other optical or infrared sensors prioritized by latency and image quality, and local observations and forecast weather conditions. ASIP data include published ice charts three times per week (Monday, Wednesday, and Friday) from 2007 – June 2014 and daily data from July 2014 – present. Prior to March 2007, ASIP published hand-drawn charts which are not included in this analysis.

WMO standard for digital ice charts stipulates that data be encoded following egg code (WMO, 1970). This methodology requires that each polygon of ice information be described by a corresponding "egg." The egg contains alphanumeric information on SIC, stage of development and thickness, and ice form and floe size. SIC information is expressed in tenths: areas with no concentration information are ice-free, a concentration value of less than one-tenth is called open water/bergy water, 1/10-3/10 indicates "very open ice", 4/10-6/10 represents "open ice", 7/10-8/10 represents "close ice", 9/10-10/10 indicates "very close ice", and a fast ice category is also encoded. For stage of development information, alpha-numeric codes correspond to different ice descriptors (e.g. Code 1 indicates new ice <10 cm, Code 6 indicates first-year ice >= 30 cm, etc.). A similar system is employed for ice form and floe size (e.g. Code 0 indicates pancake ice, Code 6 indicates vast floe (2-10 km), etc.). In this manuscript we focus only on SIC, but we note that parsing, gridding, and validating could also be done for stage/thickness and form/floe size. WMO also defines a standard color bar to indicate these concentration ranges (e.g. Fig. 1, Fig. 2). It is important to note that WMO, and in turn ASIP, call <1/10 concentration "open water/bergy bits," which is not the nomenclature that will be adopted in the remainder of this study. From this point on, open water refers to conditions where no ice is present (WMO refers to this as ice free).

On any given day, up to approximately 300 polygons are specified, with smaller, higher-resolution polygons generally near the ice edge and larger polygons within the ice pack. The daily number of polygons specified varies seasonally, with more polygons implemented in fall, winter, and spring and fewer polygons implemented in late summer, when little ice is present across the domain. Additionally, the number of polygons has steadily increased over time, coincident with an improvement in the resolution of the imagery used to generate ASIP maps. Fig. 2a,d illustrate winter and summer polygon examples. Here,

https://doi.org/10.5194/egusphere-2024-1813
Preprint. Discussion started: 20 June 2024

we choose to parse the ASIP SIC onto a 0.05° grid (in both latitude and longitude) with no interpolation. For a given ASIP polygon, each grid point that lies within its boundary is assigned that polygon's ice concentration value. The choice of 0.05° is made in order to resolve the smallest polygons, without rendering the data set too large, as there is no native grid or resolution to the polygons themselves. Polygons embedded fully within other polygons present a challenge to this gridding algorithm, as a choice must be made as to which polygon takes precedence. In this study, as in egg code, it is stipulated that a smaller polygon will always supersede a larger polygon. To obtain a single value of SIC from the range of concentrations presented in egg code, we take the average value of the range (see Fig. 2b,e), and present the range divided in half as error bars (e.g. a polygon coded as 1/10 – 3/10 ice would have 20% SIC, with 10% error bars) (see Fig 2c,f). From this point forward, ASIP will refer to our gridded SIC data set.

It is important to note that there are only 11 concentration ranges used by ASIP polygons (Table 1), which means that our gridded product also has only these 11 discrete values. Alternatively, one could imagine producing a spatially smoothed version of this dataset using a fixed or perhaps variable length scale. This is beyond the scope of this paper, as our goal here is simply to parse, grid, and validate the raw ASIP data and to compare these data with other ice concentration products. That said, if these data were to be ingested into climate models or weather forecasts, then continuous fields could be of interest.

Ice concentration range	**SIC (%)**
	0
<1/10	5
1/10 – 3/10	20
2/10 – 4/10	30
3/10 – 5/10	40
4/10 – 6/10	50
5/10 – 7/10	60
6/10 – 8/10	70
7/10 – 9/10	80
8/10 – 10/10	90
9+ (meaning >9/10	95
10 (shorefast ice only)	

Table 1: Egg code ice concentration ranges, with corresponding average SIC.

https://doi.org/10.5194/egusphere-2024-1813
Preprint. Discussion started: 20 June 2024

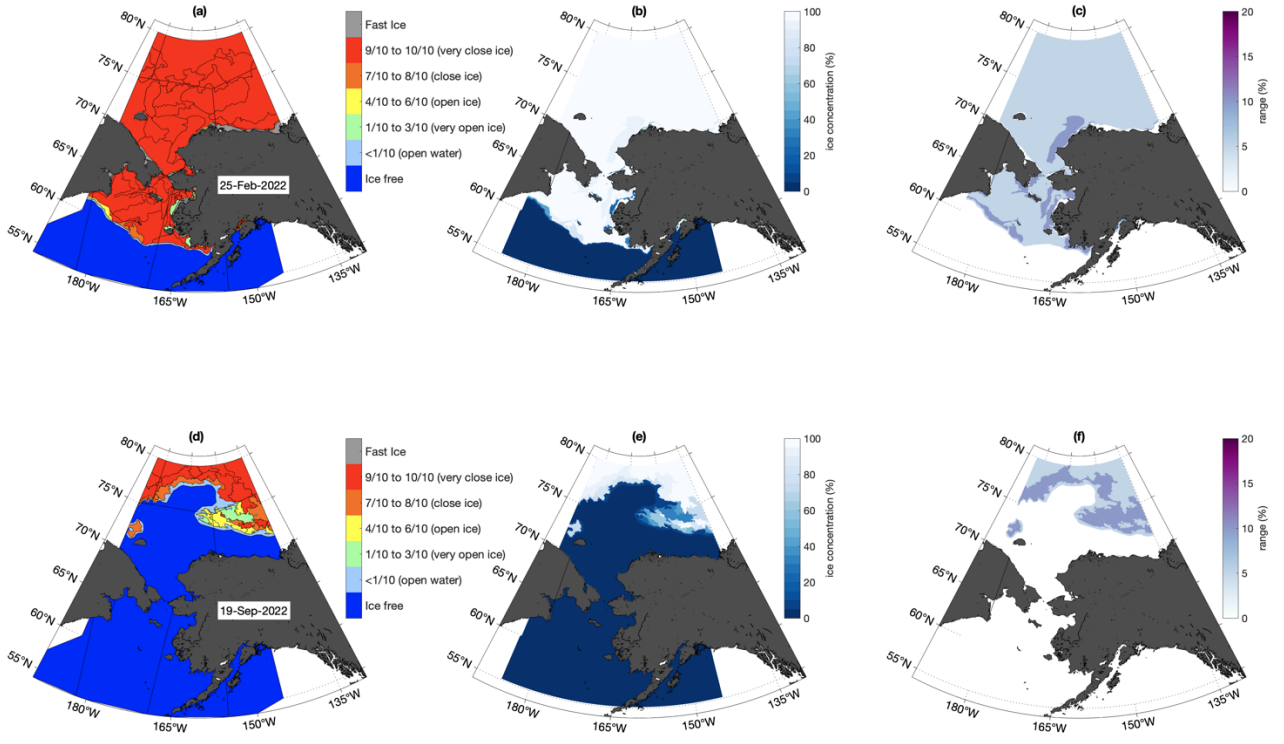

Figure 2: Example NWS ASIP polygons and resulting gridded product for winter (top row; 25 Feb, 2022) and summer (bottom row; 19 Sept, 2022) conditions. (a,d) Raw ice polygons derived from shapefiles that indicate egg code primary ice type concentration. (b,e) Gridded SIC for corresponding day, see text for details on ice concentration calculation. (c,f) SIC error bars, calculated as described in the text.

2.2 In-Situ Observations

We use a total of 5991 in-situ observations from the Pacific Arctic for the years 2007-2022, which include ship-based observations and Saildrone measurements (Table 2 and Fig. 3a). Most of these observations were collected during summer months (Fig. 3b) with a relatively even distribution among years (with the exception of 2012 and 2021, which had low sampling rates) (Fig. 3c). These in-situ observations span a range of SIC, with the majority sampling either open water or compact ice (Fig. 3d). Note that the Saildrone observations are not included in Fig. 3d, because these only provide binary ice/no ice information (Table 2) and therefore cannot be binned into concentration ranges.

Observational Platform	Dates	Observation type	Data source
CCGS Louis S. St-Laurent	26 July – 31 Aug, 2007	%	Ice Watch
CCGS Louis S. St-Laurent	17 July – 20 Aug, 2008	%	Ice Watch
CCGS Louis S. St-Laurent	17 Sept – 15 Oct, 2009	%	Ice Watch

https://doi.org/10.5194/egusphere-2024-1813
Preprint. Discussion started: 20 June 2024

CCGS Louis S. St-Laurent	15 Sept – 15 Oct, 2010	%	Ice Watch
CCGS Louis S. St-Laurent	21 July – 18 Aug, 2011	%	Ice Watch
USCGC Healy	15 Aug – 28 Sept, 2011	%	Ice Watch
CCGS Louis S St-Laurent	1 Aug – 8 Sept, 2012	%	Ice Watch
CCGS Louis S St-Laurent	1 Aug – 2 Sept, 2013	%	Ice Watch
USCGC Healy	12 May – 23 June, 2014	%	Ice Watch
CCGS Louis S. St-Laurent	21 Sept – 17 Oct, 2014	%	Ice Watch
USCGC Healy	9 Aug – 12 Oct, 2015	%	Ice Watch
CCGS Louis S. St-Laurent	18 Sept – 18 Oct, 2015	%	Ice Watch
RV Sikuliaq	1 Oct – 10 Nov, 2015	%	Ice Watch
CCGS Sir Wilfrid Laurier	1 July – 22 July, 2016	%	ArcticData
CCGS Louis S. St-Laurent	22 Sept – 16 Oct, 2016	%	Ice Watch
USCGC Healy	26 Aug – 15 Sept, 2017	%	ArcticData
RV Araon	3 Aug – 26 Aug, 2018	%	Ice Watch
CCGS Louis S. St-Laurent	5 Sept – 2 Oct, 2018	%	Ice Watch
USCGC Healy	14 Sept – 19 Oct, 2018	%	Ice Watch
Saildrones (x3)	15 May – 11 Octo, 2019	binary	Chiodi et al., 2021
CCGS Louis S. St-Laurent	12 Sept – 15 Sept, 2019	%	Ice Watch
RV Sikuliaq	7 Nov – 27 Dec, 2019	%	Ice Watch
KV Svalbard	15 Oct – 25 Nov, 2020	%	Ice Watch
Saildrones (x2)	18 June – 17 July, 2022	binary	García-Reyes et al., 2023

Table 2: In-situ observations with platform, survey duration, observation type (either binary ice/no ice or SIC), and data source.

https://doi.org/10.5194/egusphere-2024-1813
Preprint. Discussion started: 20 June 2024

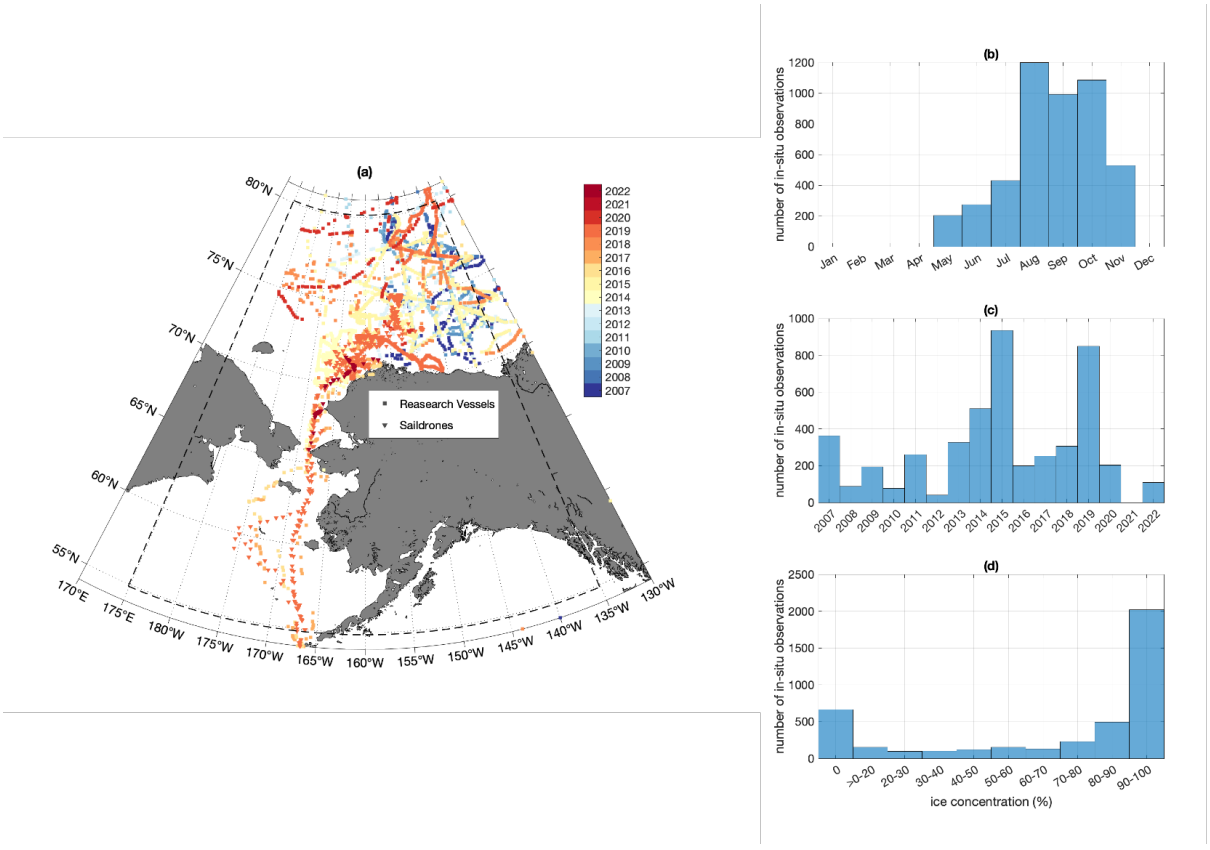

Figure 3: In-situ observations. (a) Map of in-situ observations, shaded by year of observation. (b) Histogram of seasonal distribution of in-situ observations. (c) Histogram of interannual distribution of in-situ observations. (d) Histogram of SIC distribution of in-situ observations.

2.2.1 Ship-based observations

The ship-based observations are predominantly obtained from the international Ice Watch program. This program follows Antarctic Sea Ice Processes & Climate protocol (ASPeCt) (e.g. Worby and Allison, 1999; Worby and Dirita, 1999) extended to the Arctic through the software for Arctic Shipborne Sea Ice Standardization Tool (ASSIST) (Hutchings, 2020). This program facilitates standardized collection of ship-based human observations of ice and meteorological information. Generally, Ice Watch protocol requires ice observations to be made within 1 nautical mile of the ship with 360° visibility during a 10-minute sampling window. The Ice Watch program, and the ASSIST software specifically, provide instructions for determining parameters like total ice concentration, open water amount, snow, topography, melt, and other information including ice type, thickness, and floe size. This terminology comes from ASPeCt protocol, which in turn is derived from WMO codes, and is used to maintain consistency between the hemispheres. Previous studies have utilized Ice Watch data for

https://doi.org/10.5194/egusphere-2024-1813
Preprint. Discussion started: 20 June 2024

satellite ice edge validation, especially in the Antarctic (e.g. Worby and Comiso, 2004; Bietsch et al., 2015; Kern et al., 2019; Kern et al., 2020). In this study, we utilize all Ice Watch data within the Pacific Arctic, as defined in Fig. 3, from 2007-2022 (see Table 1 for details). Worby and Comiso (2004) assess an accuracy of 5-10% for Ice Watch SIC, computed by comparing the range of estimated SIC recorded by simultaneous observations made by different observers. Unfortunately, there were not enough instances of simultaneous SIC estimates available to perform the same calculation in the Pacific Arctic. Specifically, there were no Ice Watch observations from different ships occurring within 24 hours of each other, less than 0.25° apart in latitude and longitude.

While most ship observations utilized in this study are obtained through the Ice Watch program, a few cruises conducted ice watches without reporting the data through ASSIST. As specified in Table 2, we utilize 20 Ice Watch cruises that entered the Pacific Arctic during the period of interest (2007-2022) and three cruises that reported ice data to the Arctic Data Center. Two of these cruises (CCGS Sir Wilfred Laurier 2016 and USCGC Healy 2017) provided ice concentration information through the Marine Mammal Watch that is a part of the National Science Foundation's Distributed Biological Observatory program (Moore, 2019a, Moore 2019b, Moore and Grebmeier, 2018). The final non-Ice Watch cruise followed Ice Watch observation protocol for the Study of Under Ice Blooms in the Chukchi Ecosystem program (Polashenski, 2016). For the purposes of this analysis, all in-situ SIC data are averaged onto a daily grid centered at midnight UTC, since most ice maps are valid at or near this time stamp. This avoids biasing the analysis due to ships reporting at different temporal frequencies, although it also reduces the database size and effective spatial resolution for ships transiting through the MIZ . Following Beitsch et al. 2015 and Kern et al. 2019, if a 24-hour window on a given ship has fewer than three observations, it is discarded and those data are not utilized in the intercomparison. This daily averaging reduces the number of in-situ observations to 896. All in-situ SIC observations are also converted into a binary value of ice/no ice, in order to assess the ability of ASIP, AMSR2, and MASIE to detect the simple presence or absence of ice. Further, this removes the subjectivity of human-made observations of SIC per se. Most of the following analysis uses this binary approach, with the exception of Section 3.1.2 where the original SIC values are compared.

2.2.2 Saildrones

Uncrewed Surface vehicles (USVs) facilitate the collection of high-resolution surface ocean information and meteorological parameters near the air-sea interface. In this study, we utilize two USV campaigns to the Pacific Arctic performed by Saildrones (Cokelet et al., 2015; Meinig et al., 2015; Mordy et al., 2017; Gentemann et al., 2019; García-Reyes, 2023). Saildrones are wind-driven platforms with solar-powered instrumentation. In this study, we rely on Saildrones outfitted with cameras to detect the presence or absence of ice. Readers are referred to Chiodi et al., 2021 for details on the conversion of image files to a timeseries of ice/no ice from the Saildrone tracks. We utilize the data presented in Chiodi et al., 2021 for three Saildrones

https://doi.org/10.5194/egusphere-2024-1813
Preprint. Discussion started: 20 June 2024

operating in the Pacific Arctic in 2019, and we perform the same analysis on the imagery from two Saildrones in 2022. The Saildrone data (2019 and 2022) are provided on a daily grid with binary ice/no ice information only.

2.3 Other ice concentration data sets

It is of interest to compare ASIP data with other satellite-based measurements of SIC in the region. For this analysis, we utilize a high-resolution passive microwave product (AMSR2) and an operational product from the National Snow and Ice Data Center (MASIE), both of which are used often in the scientific literature.

2.3.1 Passive microwave (AMSR2)

Advanced Microwave Scanning Radiometer 2 (AMSR2) is a passive microwave sensor onboard the JAXA Global Change Observation Mission-Water (GCOM-W1) satellite. This sensor is a follow-up to AMSR-E which was onboard the NASA satellite Aqua from 2002-2011. AMSR2 was launched in 2012 and remains operational to date. It utilizes the 89-GHz channel to obtain brightness temperatures and the Arctic radiation and turbulence interaction study (ARTIST) sea ice (ASI) algorithm (Spreen et al., 2008) to compute SIC from swath brightness data. These swaths are then gridded onto daily Arctic and Antarctic polar stereographic grids that align with the National Snow and Ice Data Center's grids (at 6.25 km and 3.125 km). In this study, we utilize daily 3.125 km data from 2012-2022 obtained from the University of Bremen data archive (https://seaice.uni-bremen.de/data/amsr2/asi_daygrid_swath/n3125/). Note that the lower-resolution AMSR2 at 25 km resolution using the NASA Team 2 algorithm (Markus et al., 2018) shown in Fig. 1a is not considered in the remainder of this analysis.

2.3.2 Multisensor product (MASIE)

Multisensor Analyzed Sea Ice Extent (MASIE) is based on an operational product from the National Ice Center (NIC). Specifically, it is generated following the Interactive Multisensor Snow and Ice Mapping System (Helfirch et al, 2007), which is a NIC operational product valid at 00:00 UTC. Similar to ASIP, human analysts consider available imagery from synthetic aperture radar, visible/infrared imagery, passive microwave, and scatterometer data to generate these maps. These binary maps of ice/no ice are generated at both 1 km and 4 km resolution and use a cut-off threshold of 40% SIC, meaning that grid cells with greater than 40% SIC are designated as having ice, and grid cells with less than 40% SIC are considered ice-free (US National Ice Center et al., 2010). In this study, we utilize daily 4 km data from 2007-present obtained from the National Snow and Ice Data Center (https://nsidc.org/data/g02186/versions/1). To match the resolution of ASIP, MASIE data are re-gridded onto a 0.05° latitude/longitude grid.

2.4 Parity analysis

We compare satellite SIC to in-situ observations to assess errors in the former, assuming the latter are accurate. For each satellite product, the grid cell nearest the in-situ observation in latitude, longitude, and time is queried. If the time gap between

https://doi.org/10.5194/egusphere-2024-1813
Preprint. Discussion started: 20 June 2024

the nearest satellite pass and the in-situ observation exceeds 12 hours, the comparison is not made. The satellite grid cell is then converted to a binary ice/no ice value and compared against the in-situ observation, also converted to a binary ice/no ice value.

Confusion matrices are a tool often used in the machine learning literature to evaluate model performance (e.g., Sammut and Webb, 2011); here we adapt the method to assess the performance of our three satellite products. Confusion matrices focus on the number of correct and incorrect matchups between two datasets; in this case, the matchups between in-situ observations (taken as truth) and satellite observations are tallied. Within these matrices, correct matchups lie along the parity (i.e., 1:1) line; incorrect matchups fall in the upper left and lower right quadrants. We thus prefer to use the term "parity analysis" in the following analysis.

3 Results

3.1 Satellite products compared with in-situ observations

3.1.1 ASIP

The parity calculation for ASIP data from 2007-2022 is presented in Fig. 4. The ASIP data are converted from SIC to a binary value by specifying that all grid cells with SIC greater than or equal to 15% are considered ice pixels, while grid cells with less than 15% SIC contain no ice. This is a common choice for defining the ice edge (Zwally et al., 1983; Cavalieri et al., 1991; Meier and Stewart, 2019), and generally falls in WMO's ice free and open water categories (see Fig. 1). We note that for this calculation, binary Saildrone camera observations of ice are taken to be SIC > 15% and thus included as a positive encounter with ice. See Section 3.1.4 for further discussion on Saildrone data use.

As shown in Fig. 4 and Table 3, ASIP correctly identifies the presence of ice with an accuracy of (548+172)/(548+172+12+20)*100 = 95.7%. ASIP overpredicts ice 1.7% of the time and under-predicts ice 2.8% of the time. Since this dataset contains more ice-free than in-ice matchups (known as a class imbalance in confusion matrices), we also report the weighted average accuracy. This is done by computing the accuracy rate for the no ice condition, which represents the specificity (or true negative rate), (Q1/(Q1+Q3)) and the accuracy rate for ice conditions, which represents the sensitivity (or true positive rate), (Q4/(Q2+Q4)) and then average these two values together. In this case, the weighted accuracy is 93.7% (Table 3).

https://doi.org/10.5194/egusphere-2024-1813
Preprint. Discussion started: 20 June 2024

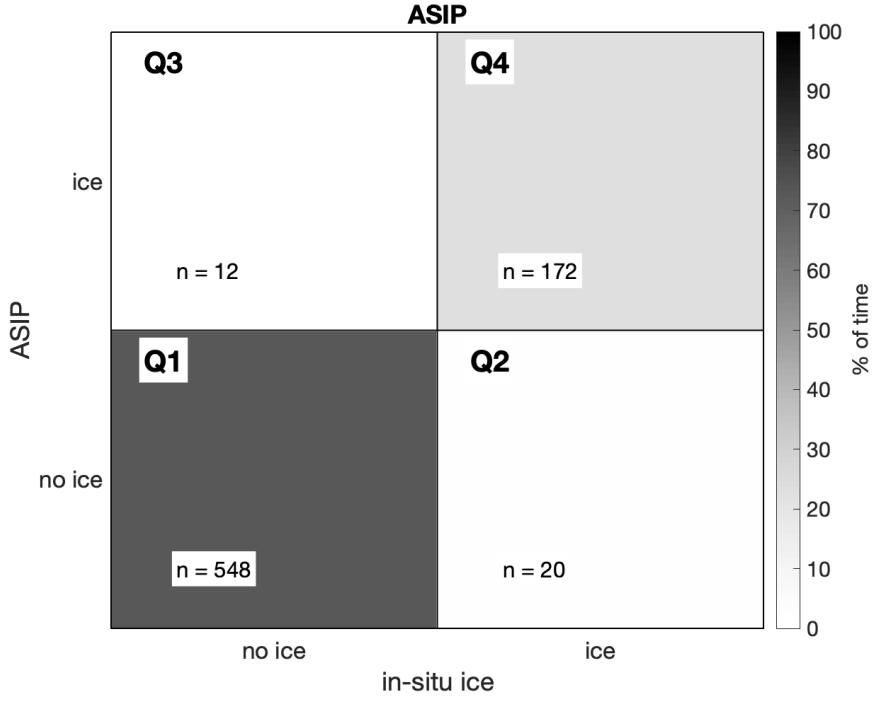

Figure 4: Full parity plot for ASIP data, 2007-2022.

	Datapoints (#)	Accuracy (%)	Weighted Accuracy (%)	Q1	Q2	Q3	Q4
ASIP	752	95.7	93.7	548	20	12	172
AMSR2	747	95.0	90.2	560	36	1	150
MASIE	301	90.7	84	50	8	20	223
ASIP vs. AMSR2	714	96.6, 95.5	95.1,89.9	547, 558	12, 31	12, 1	143, 124
ASIP vs. MASIE	228	87.3, 89.9	83, 85.3	45, 46	13, 8	16, 15	154, 159
ASIP vs. AMSR2 vs. MASIE	190	90.5, 86.8, 90.0	86.5, 89.6, 86.7	43, 54, 44	5, 23, 7	13, 2, 12	129, 111, 127
ASIP vs. AMSR2 in 0-40%	28	42.9, 21.4			16, 22		12, 6
ASIP vs. AMSR2 in 15-80%	70	55.7, 28.6			31, 50		39, 20
ASIP vs. AMSR2 in 80-100%	79	88.4, 53.2			18, 37		61, 42

Table 3: Accuracy rates and matchup counts for data combinations specified. For the 15-80% SIC range calculation, data are inclusive (i.e. data greater than or equal to 15% and less than or equal to 80% are included). The 0-40% range and the 80-100% range are non-inclusive. 0-15% range is not considered, since only 7 datapoints fall in this range.

3.1.4 ASIP, AMSR2, and MASIE

ASIP's overall accuracy rate of 95.7% is high, but to understand what that value means, it is critical to compute the corresponding accuracy rate of other products as well. To do so, AMSR2 passive microwave data and MASIE operational data are considered, and the parity calculation is re-done. In order to compare these different data sets (ASIP, AMSR2, and MASIE), we first define the intersection of all three data sets with respect to three variables: (i) years covered (i.e., 2012-2022 since

https://doi.org/10.5194/egusphere-2024-1813
Preprint. Discussion started: 20 June 2024

AMSR2 only starts in 2012), (ii) minimum SIC threshold (i.e., > 40%, from the MASIE criterion), and (iii) binary ice vs. no ice (i.e., parsing the SIC from ASIP and AMSR2 into the MASIE ice/no ice framework). These constraints result in a reduction in matchups by 75% (Table 3). A significant part of this reduction is because we have discarded Saildrone ice/no ice in-situ observations in this intercomparison, given we cannot determine the SIC > 40% threshold for these data; furthermore, the conditions encountered by the Saildrones are unlikely to be SIC > 40% because the vehicles themselves are not meant to operate in the ice. The high volume of discarded datapoints is because the Saildrone campaigns consisted of 3 vehicles in 2019 and 2 vehicles in 2022; in 2019 each of the three vehicles operated in the area for approximately 150 days (contributing approximately 450 datapoints) and in 2022 the vehicles operated for 48 and 60 days (contributing another 108 datapoints).

With these constraints, ASIP, AMSR2, and in-situ observations are converted into a binary ice/no ice by stipulating that when SIC is greater than or equal to 40%, ice is present, and when SIC is below this threshold, no ice is present. The resultant overall accuracy rates (Fig. 5 and Table 3) are similar to our original analysis for ASIP (Fig. 4), with ASIP reporting 90.5%, AMSR2 reporting 86.8% and MASIE reporting 90.0% accuracy. ASIP and MASIE tend to over-predict ice (n = 13 for ASIP and n = 12 for MASIE in Q3), whereas AMSR2 tends to underpredict ice (n= 23 in Q2). Since most in-situ observations in the subset of data queried for this calculation contain ice, these accuracy rates favor products that over-predict ice (ASIP and MASIE). The weighted accuracy rates (Table 2, calculation described in 3.1.1) reveal consistent accuracy rates among products. This overall similarity in accuracy rates (90.5% vs. 86.8% vs. 90.0%) was a surprise: given the dramatic differences in ice edge position (e.g. Fig. 1), one would expect similarly dramatic differences in accuracy rates. The lack of such differences is explained in Section 3.2.

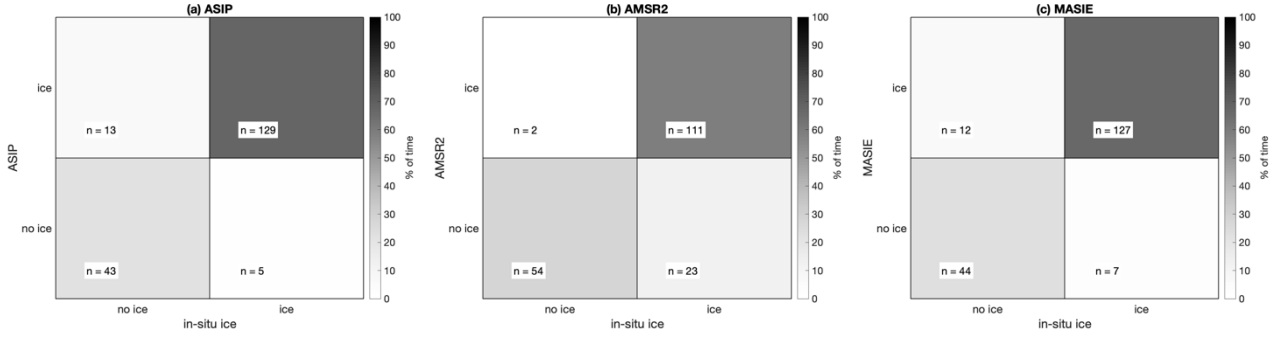

Figure 5: Parity plot for the three ice products (ASIP, AMSR2, and MASIE) combined. In-situ observations with ice concentration information (non-binary) from 2012-2022 are used. SIC cut-off is 40%.

https://doi.org/10.5194/egusphere-2024-1813
Preprint. Discussion started: 20 June 2024

3.1.2 ASIP vs. AMSR2

We now discard the SIC > 40% criterion for comparison of only ASIP and AMSR2 (but at this point keep the binary ice/no ice framework). The resulting accuracy is 96.6% for ASIP and 95.5% for AMSR2 (see Table 3 for details; weighted accuracies are 95.1% for ASIP and 89.9% for AMSR2). The primary difference between the datasets is an under-prediction of ice by AMSR2 as compared to ASIP. Specifically, while ASIP incorrectly identifies 12 in-situ observations as having no ice, when in fact ice is present, AMSR2 incorrectly identifies almost double triple that number, 31.

We now also discard the ice/no ice framework, working with the full SIC value range. Data are binned at 10% resolution (e.g. 10%-20%) except for near open water and near complete ice, which are binned at 0-5% and 95-100% (Kern et al., 2019). This is consistent with the error bars on both the in-situ values (estimated to be approximately 10%, Kern et al., 2019) and the error bars associated with converting concentration ranges to SIC values in egg code (see Fig. 2c,d). As shown in Fig. 6, for SIC < 50% ASIP tends to overpredict ice, while AMSR2 tends to underpredict ice, and both show high estimated SIC variance. This over- and under-prediction can be quantified by comparing each individual matchup for the ASIP and AMSR2 calculations. Specifically, we round all observations (in-situ, ASIP, and AMSR2) to the nearest tenth, as in Fig. 6. Subsequently, for each matchup, the residual is computed by subtracting the SIC value of the in-situ observation from the SIC value estimated by the product. A negative value indicates that the product under-predicts SIC, a positive value indicates that a product over-predicts SIC. After performing this calculation for each data matchup, the resultant residuals are summed to obtain one integrated value for each product. The results of this simple calculation indicate that AMSR2 under-predicts ice at almost double the magnitude that ASIP over-predicts ice (-1020 for AMSR2 vs. 680 for ASIP). Therefore, while neither product is perfect, the over-prediction of ice by ASIP is much smaller than the under-prediction of ice by AMSR2.

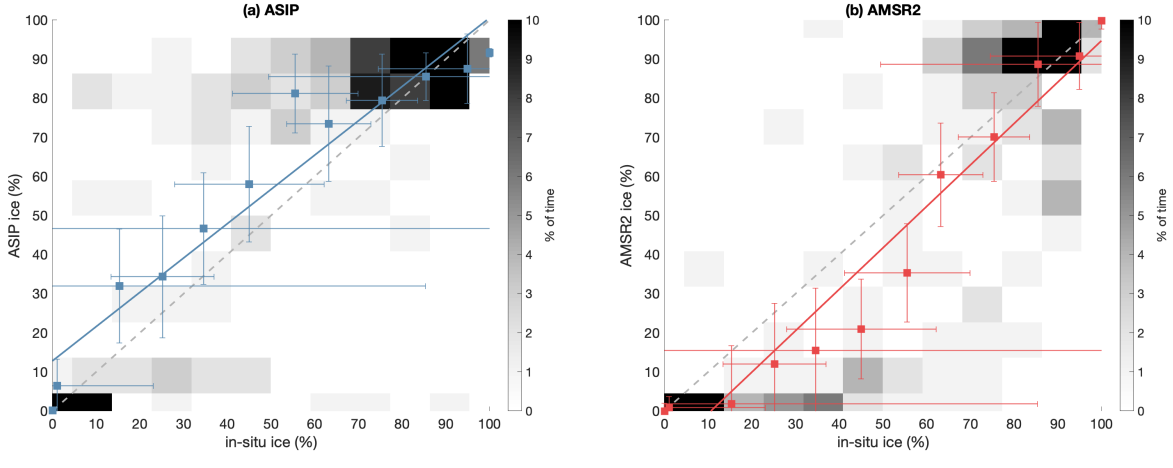

Figure 6: SIC-based parity plot for ASIP and AMSR2. Squares indicate the product average for the given in-situ concentration range (in 5% and 10% intervals, see text for details). Error bars indicate the standard deviation of the values in that bin. Solid line indicates the linear fit through the product averages. Grey dashed line indicates the 1:1 line for reference.

https://doi.org/10.5194/egusphere-2024-1813
Preprint. Discussion started: 20 June 2024

3.1.5 ASIP vs. AMSR2 within the MIZ

As described in the introduction, we seek to assess the performance of different ice products in low-ice conditions. While MASIE reports binary ice information and cannot be used to isolate specific concentration ranges, ASIP and AMSR2 data can identify the Marginal Ice Zone (MIZ), here defined to be between 15 and 80% ice concentration.

The resulting parity plot (Fig. 7) demonstrates that, although not perfect, ASIP outperforms AMSR2 in these low SIC environments. ASIP exhibits an accuracy rate of 56%, while AMSR2 exhibits an accuracy rate of 29% (a difference of 27%). Furthermore, if we do not limit the concentration reported by the product (in other words, we specify that the in-situ observations must be between 15 and 80%, but the products must simply either report or not report ice, regardless of the associated SIC value), these accuracy rates jump to 96% for ASIP (67 correct, 3 incorrect) and 73% for AMSR2 (51 correct, 19 incorrect), a difference of 23%.

However, this analysis is limited by the availability of in-situ observations within the MIZ. Recall Fig. 3d, which illustrates that the majority of in-situ observations are either in open water or in dense ice. Additionally, recall the strikingly similar accuracy rates from the parity calculations presented in Fig. 5. Both results can be explained by considering two case studies.

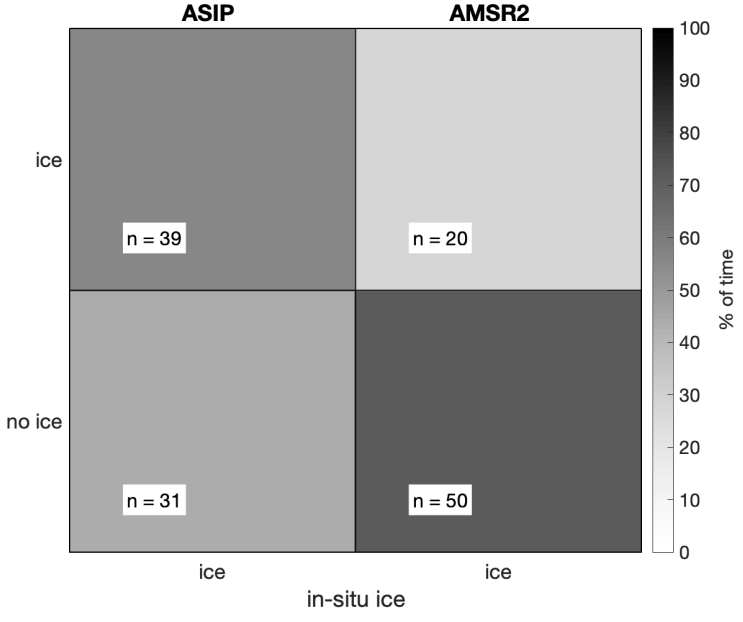

Figure 7: Parity plot for ASIP and AMSR2 within the MIZ. In-situ observations with ice concentration information (non-binary) from 2012-2022 are used. Concentration cut-offs are 15-80%, inclusive. Note the different horizontal scale used here, relative to previous parity plots: we are testing only within the MIZ, so only where in situ observations show ice.

https://doi.org/10.5194/egusphere-2024-1813
Preprint. Discussion started: 20 June 2024

3.2 Case studies

Consider the position of the in-situ asset on October 2, 2015 (Fig. 8a). The ship is far north within the pack ice, reporting a compact ice cover, and far from the ice edge regardless of which ice edge is considered. In this case, all products agree that the asset is in the ice. However, all three products disagree on the position of the ice edge (regardless of whether the ice edge is defined as the community standard of 15% or the MASIE definition of 40%). In this case study, the ASIP ice edge is further south than both the AMSR2 and MASIE ice edges, especially east of 158°W. The MASIE ice edge is similar to AMSR2 west of 152°W, but east of this longitude the MASIE ice edge is between the ASIP and AMSR2 edges. Similarly, consider the position of the in-situ asset on September 7, 2017 (Fig. 8b). The ship is far south of the ice edge, reporting open water conditions. All products agree that the ship is in open water, despite all three products reporting different ice edges. In this case study, the ASIP ice edge is systematically further south than both the AMSR2 and MASIE ice edges throughout the domain; AMSR2 and MASIE have relatively similar ice edge positions. In these two examples, while the ice edges vary dramatically between products, the in-situ assets are sampling in geographic positions and SIC ranges where the products are more likely to agree.

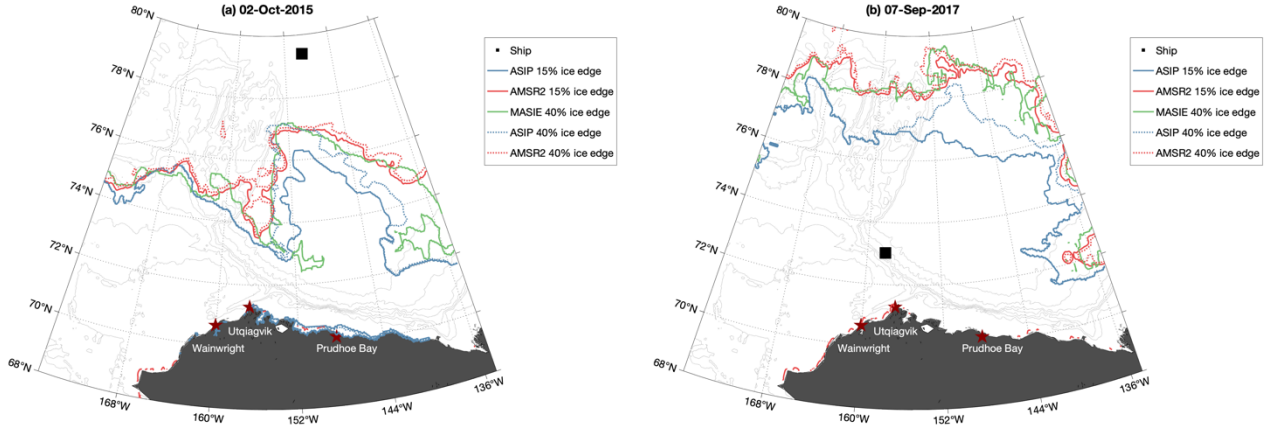

Figure 8: Two case studies that demonstrate ice edge from all three products, with both the 15% and 40% ice concentration contour plotted from ASIP and AMSR2. Black square indicates the location of the in-situ observation.

Recall the distribution of in-situ assets as a function of ice concentration (Fig. 3d), which shows that in-situ assets are predominantly found in either open water or high SIC. Thus, the in-situ observational database has a poor sampling of the MIZ, which is unfortunately exactly the region where the products most strongly disagree (Fig. 7).

https://doi.org/10.5194/egusphere-2024-1813
Preprint. Discussion started: 20 June 2024

This motivates a quantitative assessment of accuracy rates as a function of distance from the identified ice edge. To do so, the distance of each in-situ asset from the ice edge is computed. This means that each asset has three distances: a distance to the ASIP edge (15%), the AMSR2 edge (15%), and the MASIE edge (40%). These distances are then binned into 25 km ranges (requiring at least 3 datapoints per each 25 km bin), and the accuracy rate in each of these bins is computed; the results are not sensitive to the bin width chosen. The result of this calculation is shown in Fig. 9, which demonstrates that ASIP has the highest accuracy in the vicinity of its identified ice edge, followed by MASIE and lastly by AMSR2. As with the results of the MIZ parity calculation, this emphasizes the ability of ASIP to represent conditions near the ice edge more accurately than AMSR2 and MASIE.

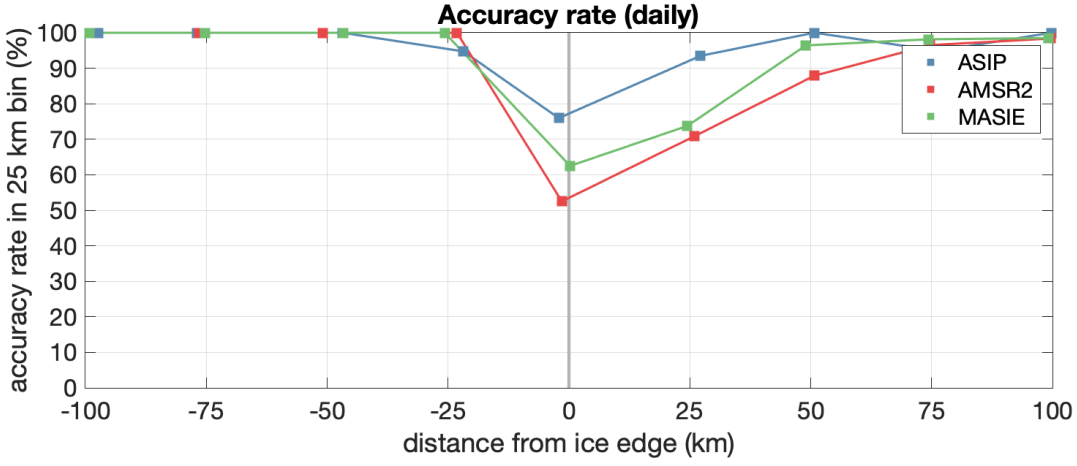

Figure 9: Binned accuracy rate as a function of distance from the ice edge, according to each product (15% for ASIP and AMSR2, 40% for MASIE). See text for details of the calculation.

3.3 Ice edge comparison

Here we present a comparison of ice edge position between satellite products. This calculation is done by first gridding AMSR2 and MASIE onto a 0.05° grid to match that of ASIP, and second by creating a land mask which is extended seaward by five pixels in each direction to remove instances of land spill over (e.g. Cavalieri et al., 1999). Additionally, masks are implemented over Wrangel and St. Lawrence Islands, and a two-dimensional 3 x 3 pixel rectangular running mean is applied to remove small-scale features. Then, for each longitude (at 0.5° resolution), the latitude of the ice edge is calculated (either 15% or 40%). Because contours can exhibit complex geometry and bisect a longitude multiple times, the latitude can be extracted in a number of ways: by finding the northernmost or southernmost crossing of the contour at a given longitude, or by plotting the contour as a function of date vs. latitude and traveling along the contour to extract the latitude nearest in time to the queried date. All three methods were implemented, and results did not differ qualitatively between methodologies. For the purposes of this

https://doi.org/10.5194/egusphere-2024-1813
Preprint. Discussion started: 20 June 2024

analysis, the date-based method is used. For each longitude, the calculation is repeated and thus results in a 2D matrix with time vs latitude information for the chosen ice concentration threshold.

This permits a comparison between ice edge location at each longitude between product pairs. For each day and for each longitude bin, the north-south distance between the two products is computed. For example, if the 15% contour in ASIP and AMSR2 is being compared, the distance between the ASIP and AMSR2 15% contour at each longitude is computed daily. The longitudinal mean is then calculated for each day, which results in a time series of ice edge distance as a function of day.

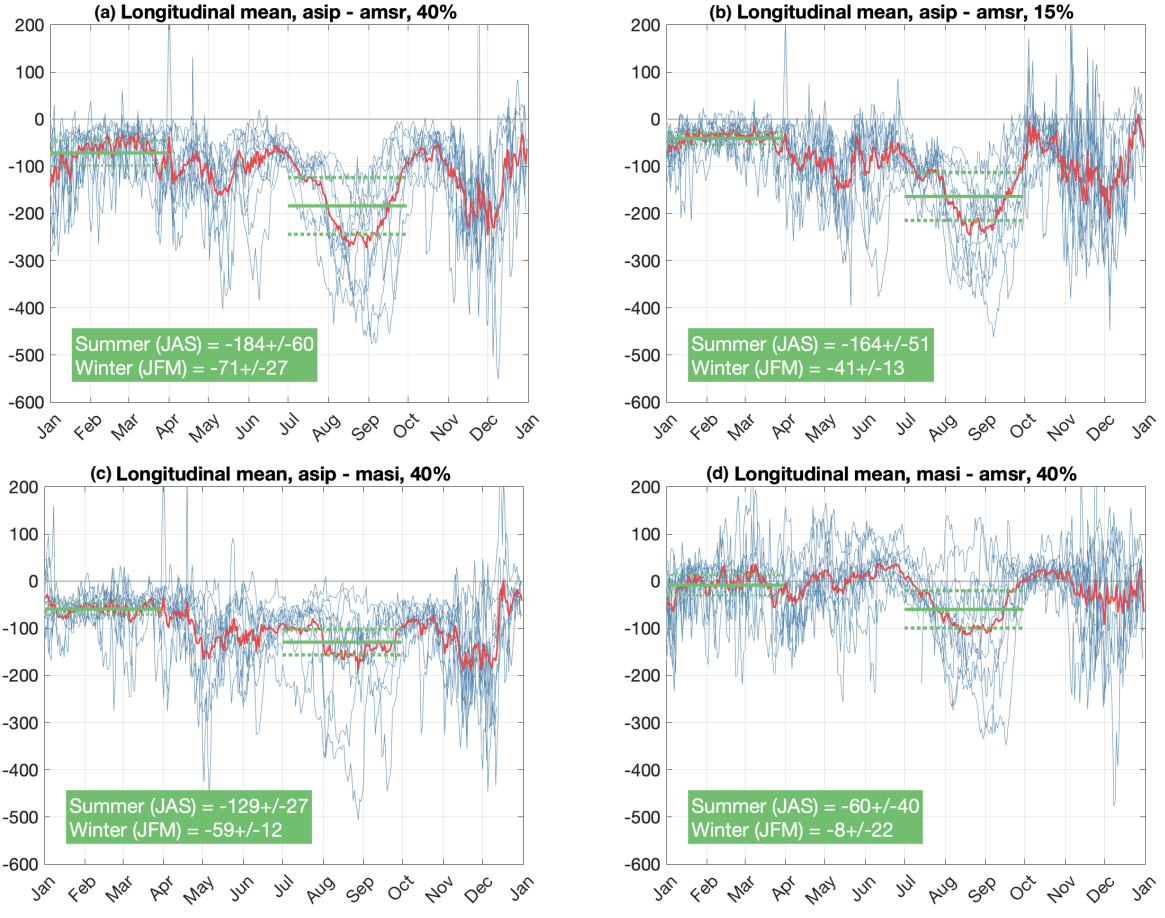

Figure 10: Distance between ice edges. (a) Longitudinal-mean distance between the ASIP and AMSR2 40% concentration contours. Blue contours represent yearly timeseries, red contour represents the mean of all years (2013-2022). (b) Same as (a) but for ASIP and AMSR2 at 15%. (c) Same as (a) but for ASIP at 40% vs. MASIE. (d) Same as (a) but for MASIE and AMSR2 at 40%. Negative values indicate that the first product (e.g. ASIP in panels a-c and MASIE in panel d) is further south than the second product. Green solid lines indicate seasonal mean (January, February, March for winter; July, August, September for Summer); green dashed lines are the standard deviation envelopes.

https://doi.org/10.5194/egusphere-2024-1813
Preprint. Discussion started: 20 June 2024

The average distance between the ASIP and AMSR2 ice edges exhibits distinct seasonal variability, with ASIP an average of 164 (184) km south of AMSR2 in summer and 41 (71) km farther south in winter for the 15% (40%) ice edges. The comparison between ASIP at 40% and MASIE demonstrates the same pattern, but with reduced distances: the ASIP ice edge is 129 km farther south in summer and 59 km farther south in winter. Finally, the MASIE ice edge is generally farther south relative to the AMSR2 ice edge in summer, but its position is not statistically different in winter.

This calculation highlights that in all cases and in all seasons, the ASIP ice edge is further south than the ice edge in AMSR2 and MASIE. Furthermore, the distance between ice edges is greater in summer than in winter in all four intercomparisons. This is likely due to the presence of melt water on the surface of the ice, as passive microwave tends to struggle when melt water is present during the summer season (e.g. Kern et al., 2020, Cavalieri et al., 1990).

4 Summary

In this study, we presented a parsed and gridded version of the National Weather Service Alaska Sea Ice Program operational ice maps. ASIP data include ice maps of the Pacific Arctic from 2007-present; for 2007-June 2014 data are provided three times per week and from July 2014-present data are reported daily. First, we detailed the parsing and gridding methodology used to convert WMO egg code ice information to maps of SIC, then we compared these SIC measurements with in-situ observations of sea ice to obtain accuracy rates, compared ASIP to a passive microwave product (AMSR2) and a second operational product (MASIE), and finally investigated the location of the ice edge in all three products.

In-situ observations of SIC from shipboard observers as part of the Ice Watch program, individual field campaigns not associated with Ice Watch, and camera measurements from autonomous vehicles provide a large dataset with which to compare the satellite measurements. ASIP performs well overall, with a 94% accuracy rate over the entire data period. When this validation exercise is computed for the lowest common denominator between ASIP, AMSR2, and MASIE, we find that generally, all products perform similarly and well, with approximately 90% accuracy rates. However, this becomes more nuanced when considering higher-order variables like SIC, instead of presence/absence of ice. The accuracy statistics reported through this method are skewed by the geographic positions of the in-situ observations, as the accuracy results report the certainty of heavy ice or open water conditions, and relatively few MIZ observations are available. In the MIZ, ASIP

https://doi.org/10.5194/egusphere-2024-1813
Preprint. Discussion started: 20 June 2024

outperforms AMSR2 (and MASIE does not have a MIZ). ASIP predicts an ice edge that is consistently further south than both the AMSR2 and MASIE ice edges throughout the Pacific Arctic, especially during the summer months when ice is melting.

5 Discussion

In most of this study, a presence/absence of ice framework was used; however, when the SIC values are retained, there is evidence that ASIP performs better than AMSR2 in most concentration ranges and especially within the MIZ (Fig. 7). At low SIC, both ASIP and AMSR2 show high estimated SIC variance, with ASIP systematically over-predicting SIC and AMSR2 under-predicting SIC (Fig. 6). However, the under-prediction in AMSR2 is double the over-prediction in ASIP, illustrating that while neither product is perfect, ASIP outperforms AMSR2 and, in an integrated framework, exhibits smaller deviations in estimated SIC from observed SIC than AMSR2 does. That said, in-situ observations of the MIZ are lacking (see Fig. 3d), indicating that there is a clear need for measurements of SIC in this subdomain. We hypothesize based on the results of the parity analysis and the calculation of product accuracy rates as a distance to the ice edge, that more in-situ observations of the MIZ might change the accuracy statistics presented here. More MIZ observations might highlight the ability for ASIP to capture this subdomain where AMSR2 tends to struggle. As shown in the case study in Fig. 1, the ASIP ice edge not only displays higher-resolution structure than the other ice edges, but also is more accurate than the other ice edges. The concept of an ice edge is dependent on the chosen threshold (e.g. 15%, 40%) and is not a simple zonal line across a given latitude. Reducing the ice edge to a smoothed contour at a given threshold removes the higher-order variability in this region that inherently characterizes the concept of an ice edge and the MIZ more generally. As a pilot navigating a vessel or an ROV near the ice edge, it is critically important to know where there are patches of heavier and lighter ice and what the shape of those distributions is across space. Since the original ASIP product is not provided on a fixed spatial grid, it is better able to represent the inherent high-order curvature in ice edges when compared to AMSR2 and MASIE. A related example of this from the sea surface temperature (SST) community is NASA's Multi-scale Ultra-high Resolution global, gridded SST product, which uses a high-resolution (0.01º) grid and multi-scale analysis to preserve small-scale features where they have been observed (Chin et al., 2017).

Matchups within the MIZ can be quite problematic, for a variety of reasons. Despite the 5-10% error bars presented by Worby and Cosimo (2004) for the Ice Watch in-situ observations, it is important to recall that this is for a 1 nautical mile radius around a ship, dependent on both the observer and the visibility at that time. This surveyed region is only a small portion of a satellite grid cell, which makes matching up the ship-based estimate with satellite estimates challenging. This is especially true in low SIC environments, where small-scale ice floes and features dominate the pixel. As such, if a ship is moored to a floe (which is often the case during on-ice buoy deployments or long-term drifts), it will sample heavier ice conditions than the broader pixel. Conversely, most ships will preferentially navigate through leads or low ice regions, potentially biasing the in-situ observations to low values. Furthermore, taking daily averages of ship position and SIC

https://doi.org/10.5194/egusphere-2024-1813
Preprint. Discussion started: 20 June 2024

complicate this calculation, as a ship is more likely to move across a large range of SIC measurements in one day when in the MIZ than when in heavy ice, because a ship can move faster in low SIC conditions than when backing and ramming in high SIC environments. As such, the ship may transit from 15% to 50% to 100% ice in one day, and these values would average to 55% ice cover, despite the fact that at the time of satellite passage, the ship may be closer to the low or high ends of this range.

Despite these limitations, it is evident that more in-situ observations of the MIZ are needed and would likely impact the results of our parity analysis. The results of this study, both ASIP validation and the intercomparison between ASIP and AMSR2 and MASIE, indicate that ASIP is a valuable product to include in scientific analysis of ice conditions, especially in low SIC environments, during periods of active melt, and when isolating a high-resolution ice edge.

We note that our gridded ASIP SIC product provides a relatively accurate field (compared to in situ observations) and thus can be used as an optimal "state estimate" of SIC in the Pacific Arctic on any given day. This should be useful for a variety of scientific studies, including numerical model validation. However, as noted previously, ASIP inputs, analysis methods, and human analysts change over time, and thus this product likely should not be used for long-term sea ice climate studies.

Competing Interests

The authors declare that they have no conflict of interest.

Author contribution

AP and MS formulated the study. AP wrote the code, performed the analysis, and drafted the manuscript. All authors advised on the methodology and the interpretation of findings. All authors reviewed and edited the manuscript.

Acknowledgements

The authors thank the captains, crews, and observers onboard all 23 cruises utilized in this analysis. The authors thank the NOAA Saildrone mission teams from 2019 and 2022 for successful missions, especially Andrew Chiodi and Marisol García-Reyes for providing access to the data. We are grateful to all ice analysts at ASIP and MASIE who contributed to the ice maps over the years, and we acknowledge Harry Stern, Melinda Webster, and Axel Schweiger for useful discussions. A.P. was funded by NSF OPP-2219147. M.S. was funded by NSF OPP-1751363, ONR N00014-21-1-2868, and NASA 80NSSC18K0837 and 80NSSC21K0832.

https://doi.org/10.5194/egusphere-2024-1813
Preprint. Discussion started: 20 June 2024

Code Availability

The codes used to parse, project, and grid the National Weather Service Alaska Sea Ice Program are available on GitHub at https://github.com/astridpacini/NWS_ASIP. The Climate Data Toolbox for MATLAB (Greene et al., 2019) was utilized to compute land masks.

Data Availability

The AMSR2 data at 3.125 km resolution were downloaded from the University of Bremen at https://data.seaice.uni-bremen.de/amsr2/asi_daygrid_swath/n3125/. AMSR2 at 25 km resolution were downloaded from the National Snow and Ice Data Center at https://nsidc.org/data/au_si25/versions/1. MASIE data are also available for download from the National Snow and Ice Data Center at https://nsidc.org/data/g02186/versions/1#anchor-1. ASIP ice charts were provided by ASIP analysts and are available upon request via email at nws.ar.ice@noaa.gov. All Ice Watch data were downloaded from the Ice Watch data repository at https://icewatch.met.no/about. The two DBO cruises utilized in this study were obtained from the Arctic Data Center (CCGS Sir Wilfed Laurier 2016 cruise: https://arcticdata.io/catalog/view/doi%3A10.18739%2FA27P8TD2J; USCGC Healy 2017 cruise: https://arcticdata.io/catalog/view/doi%3A10.18739%2FA25Q4RM2M). The data from the Study of Under Ice Blooms in the Chukchi Ecosystem USCGC Healy 2014 cruise were obtained from the Arctic Data Center at https://arcticdata.io/catalog/view/doi%3A10.18739%2FA2416T03D.

References

Agnew, T. and Howell, S.: The use of operational ice charts for evaluating passive microwave ice concentration data, Atmosphere - Ocean, 41, 317–331, https://doi.org/10.3137/ao.410405, 2003.

Armstrong, T.: World Meteorological Organization. WMO sea-ice nomenclature. Terminology, codes and illustrated glossary. Edition 1970. Geneva, Secretariat of the World Meteorological Organization, 1970. [ix], 147 p. [including 175 photos] + corrigenda slip. (WMO/OM- M/BMO, No. 259, TP. 145.), Journal of Glaciology, 11, 148–149, https://doi.org/10.3189/s0022143000022577, 1972.

Beitsch, A., Kern, S., and Kaleschke, L.: Comparison of SSM/I and AMSR-E sea ice concentrations with ASPeCt ship observations around antarctica, IEEE Transactions on Geoscience and Remote Sensing, 53, 1985–1996, https://doi.org/10.1109/TGRS.2014.2351497, 2015.

Boylan, B. M.: Increased maritime traffic in the Arctic: Implications for governance of Arctic sea routes, Marine Policy, 131, https://doi.org/10.1016/j.marpol.2021.104566, 2021.

Cavalieri, D. J., Gloersen, P., and Campbell, W. J.: Determination of sea ice parameters with the Nimbus 7 SMMR., Journal of Geophysical Research, 89, 5355–5369, https://doi.org/10.1029/JD089iD04p05355, 1984.

https://doi.org/10.5194/egusphere-2024-1813
Preprint. Discussion started: 20 June 2024

Cavalieri, D. J., Burns, B. A., and Onstott, R. G.: Investigation of the effects of summer melt on the calculation of sea ice concentration using active and passive microwave data, Journal of Geophysical Research, 95, 5359–5369, https://doi.org/10.1029/JC095iC04p05359, 1990.

Center, U. N. I., Snow, N., Center, I. D., by F. Fetterer, C., Savoie, M., Helfrich, S., and Clemente-Col{ó}n, P.: Multisensor Analyzed Sea Ice Extent - Northern Hemisphere (MASIE-NH), Version 1, 2010.

Chin, T. M., Vazquez-Cuervo, J., and Armstrong, E. M.: A multi-scale high-resolution analysis of global sea surface temperature, https://doi.org/10.5067/GHGMR-4FJ04, 2017.

Chiodi, A. M., Zhang, C., Cokelet, E. D., Yang, Q., Mordy, C. W., Gentemann, C. L., Cross, J. N., Lawrence-Slavas, N., Meinig, C., Steele, M., Harrison, D. E., Stabeno, P. J., Tabisola, H. M., Zhang, D., Burger, E. F., O'Brien, K. M., and Wang, M.: Exploring the Pacific Arctic Seasonal Ice Zone With Saildrone USVs, Frontiers in Marine Science, 8, 1–20, https://doi.org/10.3389/fmars.2021.640697, 2021.

Cokelet, E. D., Meinig, C., Lawrence-Slavas, N., Stabeno, P. J., Mordy, C. W., Tabisola, H. M., Jenkins, R., and Cross, J. N.: The Use of Saildrones to Examine Spring Conditions in the Bering Sea: Instrument Comparisons, Sea Ice Meltwater and Yukon River Plume Studies, 2015.

Comiso, J. C.: Characteristics of Arctic winter sea ice from satellite multispectral microwave observations., Journal of Geophysical Research, 91, 975–994, https://doi.org/10.1029/JC091iC01p00975, 1986.

Comiso, J. C. and Kwok, R.: Surface and radiative characteristics of the summer Arctic sea ice cover from multisensor satellite observations, Journal of Geophysical Research: Oceans, 101, 28 397–28 416, https://doi.org/10.1029/96JC02816, 1996.

Comiso, J. C. and Nishio, F.: Trends in the sea ice cover using enhanced and compatible AMSR-E, SSM/I, and SMMR data, Journal of Geophysical Research: Oceans, 113, https://doi.org/10.1029/2007JC004257, 2008.

Council, A.: Arctic Marine Shipping Assessment 2009 Report, 2009.

Deemer, G. J., Bhatt, U. S., Eicken, H., Posey, P. G., Hutchings, J. K., Nelson, J., Heim, R., Allard, R. A., Wiggins, H., and Creek, K.: Broadening the sea-ice forecaster toolbox with community observations: A case study from the northern Bering Sea, Arctic Science, https://doi.org/10.1139/as-2016-0054, 2017.

Drushka, K., Westbrook, E., Bingham, F. M., Gaube, P., Dickinson, S., Fournier, S., Menezes, V., Misra, S., Perez, J., Rainville, E. J., Schmidgall, C., Shcherbina, A., Steele, M., Thomson, J., and Zippel, S.: Salinity and Stratification at the Sea Ice Edge (SASSIE): An oceanographic field campaign in the Beaufort Sea, Earth System Science Data, https://doi.org/10.5194/essd-2023-406, 2024. Fox

Kemper, B., Hewitt, H., Xiao, C., et. al., and on Climate Change, I. P.: Ocean, Cryosphere and Sea Level Change, pp. 1211–1362, Cambridge University Press, https://doi.org/10.1017/9781009157896.011, 2021.

García-Reyes, M., Minnett, P. J., Steele, M., Castro, S., Cornillon, P., Armstrong, E., Vazquez-Cuervo, J., Tsontos, V., Cokelet, E., and Wick, G. A.: 2022 Arctic Saildrone Cruise Report, 2023.

Gentemann, C. L., Minnett, P., Steele, M., Castro, S., Cornillon, P., Armstrong, E., Vazquez, J., Tsontos, V., and Cokelet, E.: 2019 Arctic Saildrone Cruise Report (Version 1), https://doi.org/10.5281/zenodo.5851764, 2019.

https://doi.org/10.5194/egusphere-2024-1813
Preprint. Discussion started: 20 June 2024

Gogineni, S. P., Moore, R. K., Grenfell, T. C., Barber, D. G., Digby, S., and Drinkwater, M.: The effects of freeze-up and melt processes on microwave signatures, pp. 329–341, https://doi.org/10.1029/GM068p0329, 1992.

Greene, C. A., Thirumalai, K., Kearney, K. A., Delgado, J. M., Schwanghart, W., Wolfenbarger, N. S., Thyng, K. M., Gwyther, D. E., Gardner, A. S., and Blankenship, D. D.: The Climate Data Toolbox for MATLAB, Geochem. Geophy. Geosy., 2

Grenfell, T. C. and Lohanick, A. W.: Temporal variations of the microwave signatures of sea ice during the late spring and early summer near Mould Bay NWT., Journal of Geophysical Research, 90, 5063–5074, https://doi.org/10.1029/JC090iC03p05063, 1985.

Haine, T. W. and Martin, T.: The Arctic-Subarctic sea ice system is entering a seasonal regime: Implications for future Arctic amplification, Scientific Reports, 7, https://doi.org/10.1038/s41598-017-04573-0, 2017.

Heim, R. and Schreck, M.: NWS Alaska Sea Ice Program: Operations, Customer Support and Challenges, 2017.

Helfrich, S. R., McNamara, D., Ramsay, B. H., Baldwin, T., and Kasheta, T.: Enhancements to, and forthcoming developments in the Interactive Multisensor Snow and Ice Mapping System (IMS), Hydrological Processes, 21, 1576–1586, https://doi.org/10.1002/hyp.6720, 2007.

Hufford, G.: National Weather Service Alaska Region Sea Ice Program, 2009.

Hutchings, J., Delamere, J., and Heil, P.: The Ice Watch Manual, https://icewatch.met.no., 2020.

Ivanova, N., Pedersen, L. T., Tonboe, R. T., Kern, S., Heygster, G., Lavergne, T., Sørensen, A., Saldo, R., Dybkjær, G., Brucker, L., and

Shokr, M.: Inter-comparison and evaluation of sea ice algorithms: Towards further identification of challenges and optimal approach using passive microwave observations, Cryosphere, 9, 1797–1817, https://doi.org/10.5194/tc-9-1797-2015, 2015.

Kern, S., Lavergne, T., Notz, D., Pedersen, L. T., Tonboe, R. T., Saldo, R., and Sørensen, A. M.: Satellite passive microwave sea-ice concentration data set intercomparison: Closed ice and ship-based observations, Cryosphere, 13, 3261–3307, https://doi.org/10.5194/tc-13-3261- 2019, 2019.

Kern, S., Lavergne, T., Notz, D., Pedersen, L. T., and Tonboe, R.: Satellite passive microwave sea-ice concentration data set inter-comparison for Arctic summer conditions, Cryosphere, 14, 2469–2493, https://doi.org/10.5194/tc-14-2469-2020, 2020.

Kwok, R. and Rothrock, D. A.: Decline in Arctic sea ice thickness from submarine and ICESat records: 1958-2008, Geophysical Research Letters, 36, https://doi.org/10.1029/2009GL039035, 2009.

Lindsay, R. and Schweiger, A.: Arctic sea ice thickness loss determined using subsurface, aircraft, and satellite observations, Cryosphere, 9, 269–283, https://doi.org/10.5194/tc-9-269-2015, 2015.

Markus, T. and Dokken, S. T.: Evaluation of Late Summer Passive Microwave Arctic Sea Ice Retrievals, 2002.

Markus, T., Comiso, J. C., and Meier, W. N.: AMSR-E/AMSR2 Unified L3 Daily 25 km Brightness Temperatures and Sea Ice Concentration Polar Grids, Version 1, https://doi.org/10.5067/TRUIAL3WPAUP, 2018.

https://doi.org/10.5194/egusphere-2024-1813
Preprint. Discussion started: 20 June 2024

Meier, W. and Notz, D.: A note on the accuracy and reliability of satellite-derived passive microwave estimates of sea-ice extent, CliC Arctic sea ice working group consensus document, World Climate Research Program, 2010

Meier, W. N. and Markus, T.: Remote sensing of sea ice, pp. 248–272, wiley, ISBN 9781118368909, https://doi.org/10.1002/9781118368909.ch11, 2014.

Meier, W. N., Fetterer, F., Stewart, J. S., and Helfrich, S.: How do sea-ice concentrations from operational data compare with passive microwave estimates? Implications for improved model evaluations and forecasting, Annals of Glaciology, 56, 332–340, https://doi.org/10.3189/2015AoG69A694, 2015.

Meinig, C., Jenkins, R., Lawrence-Slavas, N., and Tabisola, H.: The Use of Saildrones to Examine Spring Conditions in the Bering Sea: vehicle specification and mission performance, 2015.

Moore, S.: Marine Mammal Watch, Northern Bering Sea and Chukchi Sea, July, 2016, 2019a.

Moore, S.: Marine Mammal Watch, Northern Bering Sea and Chukchi Sea, August-September, 2017, 2019b.

Moore, S. E. and Grebmeier, J. M.: The Distributed Biological Observatory, Arctic Observing Summit, 71, 1–7, https://doi.org/10.2307/26646184, 2018.

Mordy, C. W., Cokelet, E. D., Robertis, A. D., Jenkins, R., Kuhn, C. E., Lawrence-Slavas, N., Berchok, C. L., Crance, J. L., Sterling, J. T., Cross, J. N., Stabeno, P. J., Meinig, C., Tabisola, H. M., Burgess, W., and Wangen, I.: Advances in Ecosystem Research: Saildrone Surveys of Oceanography, Fish, and Marine Mammals in the Bering Sea, Oceanography, 30, 113–115, https://doi.org/10.2307/26201857, 2017. Organization, W. M.: WMO sea-ice nomenclature. Terminology, codes, and illustrated glossary, 1970.

Perovich, D., Meier, W., Tschudi, M., Hendricks, S., Petty, A. A., Divine, D., Farrell, S., Gerland, S., Haas, C., Kaleschke, L., Pavlova, O., Ricker, R., Tian-Kunze, X., Webster, M., and Wood, K.: NOAA Arctic Report Card 2020, https://doi.org/10.25923/n170-9h57, 2020.

Polashenski, C.: Underway Sea Ice Observations during SUBICE 2014, 2016.

Rösel, A., Kaleschke, L., and Birnbaum, G.: Melt ponds on Arctic sea ice determined from MODIS satellite data using an artificial neural network, Cryosphere, 6, 431–446, https://doi.org/10.5194/tc-6-431-2012, 2012.

Sammut, C. and Webb, G. I., eds.: Encyclopedia of Machine Learning, Springer Science {&} Business Media, 2011.

Serreze, M. C. and Stroeve, J.: Arctic sea ice trends, variability and implications for seasonal ice forecasting, Philosophical Transactions of the Royal Society A: Mathematical, Physical and Engineering Sciences, 373, https://doi.org/10.1098/rsta.2014.0159, 2015.

Spreen, G., Kaleschke, L., and Heygster, G.: Sea ice remote sensing using AMSR-E 89-GHz channels, Journal of Geophysical Research: Oceans, 113, https://doi.org/10.1029/2005JC003384, 2008.

https://doi.org/10.5194/egusphere-2024-1813
Preprint. Discussion started: 20 June 2024

Steffen, K. and Schweiger, A.: NASA team algorithm for sea ice concentration retrieval from Defense Meteorological Satellite Program special sensor microwave imager: comparison with Landsat satellite imagery, Journal of Geophysical Research, 96, https://doi.org/10.1029/91jc02334, 1991.

Thomson, J.: SASSIE Arctic Field Campaign Wave Glider Data Fall 2022. Ver. 1, 2023.

Thomson, J., Girton, J. B., Jha, R., and Trapani, A.: Measurements of directional wave spectra and wind stress from a Wave Glider autonomous surface vehicle, Journal of Atmospheric and Oceanic Technology, 35, 347–363, https://doi.org/10.1175/JTECH-D-17-0091.1, 2018.

Vazquez-Cuervo, J., Castro, S. L., Steele, M., Gentemann, C., Gomez-Valdes, J., and Tang, W.: Comparison of GHRSST SST Analysis in the Arctic Ocean and Alaskan Coastal Waters Using Saildrones, Remote Sensing, 14, https://doi.org/10.3390/rs14030692, 2022.

Worby, A. P. and Allison, I.: A technique for making ship-based observations of Antarctic sea ice thickness and characteristics, Part I Observational Technique and Results, 1999.

Worby, A. P. and Comiso, J. C.: Studies of the Antarctic sea ice edge and ice extent from satellite and ship observations, Remote Sensing of Environment, 92, 98–111, https://doi.org/10.1016/j.rse.2004.05.007, 2004.

Worby, A. P. and Dirita, V.: A technique for making ship-based observations of Antarctic sea ice thickness and characteristics, Part 2 User operating manual, 1999.